Small unilamellar vesicles: a platform technology for molecular imaging of brain tumors

2011 Nanotechnology 22 195102

(http://iopscience.iop.org/0957-4484/22/19/195102)

Nanotechnology **22** (2011) 195102 (15pp) doi:10.1088/0957-4484/22/19/195102

Small unilamellar vesicles: a platform technology for molecular imaging of brain tumors

Umar Iqbal[1], Homam Albaghdadi[1], Mu-Ping Nieh[2,3], Ursula I Tuor[4], Zoltan Mester[5], Danica Stanimirovic[1], John Katsaras[2,6] and Abedelnasser Abulrob[1]

[1] Institute for Biological Sciences, National Research Council of Canada, 1200 Montreal Road, Ottawa, ON, K1A 0R6, Canada
[2] Canadian Neutron Beam Centre, Chalk River Laboratories, National Research Council Canada, Chalk River, ON, K0J 1J0, Canada
[3] Department of Chemical, Materials and Biomolecular Engineering, Institute of Materials Science, University of Connecticut, Storrs, CT 60269-3136, USA
[4] Institute for Biodiagnostics (West), National Research Council of Canada, B153-3330 Hospital Drive NW, Calgary, AB, T2N 4N1, Canada
[5] Institute for National Measurements Standards, National Research Council Canada, Ottawa, ON, K1A 0R6, Canada
[6] Oak Ridge National Laboratory, Neutron Scattering Sciences Division, Oak Ridge, TN, USA

E-mail: Abedelnasser.abulrob@nrc.gc.ca

Received 25 November 2010, in final form 1 March 2011
Published 24 March 2011
Online at stacks.iop.org/Nano/22/195102

Abstract
Molecular imaging enables the non-invasive investigation of cellular and molecular processes. Although there are challenges to overcome, the development of targeted contrast agents to increase the sensitivity of molecular imaging techniques is essential for their clinical translation. In this study, spontaneously forming, small unilamellar vesicles (sULVs) (30 nm diameter) were used as a platform to build a bimodal (i.e., optical and magnetic resonance imaging (MRI)) targeted contrast agent for the molecular imaging of brain tumors. sULVs were loaded with a gadolinium (Gd) chelated lipid (Gd-DPTA-BOA), functionalized with targeting antibodies (anti-EGFR monoclonal and anti-IGFBP7 single domain), and incorporated a near infrared dye (Cy5.5). The resultant sULVs were characterized *in vitro* using small angle neutron scattering (SANS), phantom MRI and dynamic light scattering (DLS). Antibody targeted and nontargeted Gd loaded sULVs labeled with Cy5.5 were assessed *in vivo* in a brain tumor model in mice using time domain optical imaging and MRI. The results demonstrated that a spontaneously forming, nanosized ULVs loaded with a high payload of Gd can selectively target and image, using MR and optical imaging, brain tumor vessels when functionalized with anti-IGFBP7 single domain antibodies. The unique features of these targeted sULVs make them promising molecular MRI contrast agents.

1. Introduction

Molecular imaging enables the simultaneous anatomical localization and quantitative evaluation of target biomolecules that can guide the selection of treatment protocols, and whose efficacy can also be quantified. The expected impact of these technologies in reducing the drug development cycle has been emphasized in the US Foods and Drugs Administration's (FDA) 'Critical Path Initiative', which recommends the 'integration of molecular and imaging biomarkers into every stage of the regulatory review for drug, diagnostic, and biologic applications' (Woodcock and Woosley 2008). Currently, there are only a limited number of molecular imaging agents suitable for clinical applications (Cai and Chen 2008).

Most molecular imaging applications for cancer have been developed for radioactivity dependent positron emission tomography (PET) and single photon emission computed tomography (SPECT) modalities (Michalski and Chen 2010). However, similar compounds are presently lacking for the more accessible magnetic resonance imaging (MRI) modality, as well as for the rapidly developing and cheaper optical imaging modality (Pan *et al* 2010). MRI is a non-invasive and powerful medical diagnostic technique that offers high-resolution anatomical information, and is frequently used for the non-invasive detection of a variety of diseases (De Schepper and Bloem 2007). MRI creates images of the body using the principles of nuclear magnetic resonance. Images are usually generated with Gd (Gd-DTPA) as a contrast agent, based on its free distribution in the body. While these images provide good anatomical information about disease (e.g., tumors) localization and spread, to obtain information about molecular characteristics of the disease (e.g., expression of certain receptors that relate to disease prognosis, progression, etc), a targeted contrast agent approach is required (Glunde *et al* 2007). The clinical translation of these imaging agents will depend, however, on the development of new targeted contrast agents functionalized against disease-specific biomarkers that have been validated in animal models. Moreover, such systems should ideally lend themselves to be fabricated at reasonable cost. Current Gd contrast agents (i.e. Gd-DPTA or Magnevist®) on the market require tissue concentrations of between 1 and 100 mM in order to obtain good quality image contrast (Gupta and Weissleder 1996). To overcome sensitivity issues, the use of liposomes capable of carrying a high payload of Gd has been suggested as a viable strategy (Glogard *et al* 2002). A variety of targeted contrast agents consisting of Gd loaded liposomes functionalized with targeting peptides or antibodies have been developed to date (Mulder *et al* 2005, Zhang *et al* 2009, Strijkers *et al* 2010). However, the clinical use of Gd loaded liposomes has been hampered by slow clearance and detection sensitivity (Xu *et al* 2007, Zhang *et al* 2009).

Monodisperse (uniform size) liposomes are often produced using a costly multistage filtration or extrusion process that breaks up the multi-lamellar structure that naturally forms in many commonly used lipid mixtures. Recently, we reported that a long- and short-chain phospholipid mixture (e.g., dimyristoyl phosphatidylcholine, DMPC, and dihexanoyl phosphatidylcholine, DHPC, respectively), doped with a long-chain charged lipid (dimyristoyl phosphatidylglycerol, DMPG) spontaneously forms small unilamellar vesicles (sULV) with a low-polydispersity (Nieh *et al* 2003, 2004, 2005). The size (diameter) of these sULVs ranges from 10 to 40 nm, and can be obtained in a controlled manner without multistage filtration (Nieh *et al* 2003, 2004, Yue *et al* 2005). sULVs have also been shown to encapsulate molecules (Nieh *et al* 2008). In short, compared to traditional extrusion methods, sULVs offer the distinct advantage of reducing manufacturing costs and extending product shelf life.

Epidermal growth factor receptor (EGFR) and insulin-like-growth-factor binding protein 7 (IGFBP7) are two targets that are overexpressed in brain tumor cells or brain tumor vessels, respectively (Iqbal *et al* 2010b, 2010a). The targeting moiety, anti-EGFR monoclonal antibody (mAb) linked to liposomes has been used previously to target EGFR-overexpressing tumor cells in a xenograft brain tumor model (Mamot *et al* 2005). The xenograft tumor model was used due to the presence of 'leaky' vasculature, which allowed access of the EGFR targeted liposome to the tumor cells. In comparison, anti-IGFBP7 single domain antibodies (sdAbs) have been used previously to selectively bind to brain tumor vessels *in vivo* in a more relevant orthotopic brain tumor model (Iqbal *et al* 2010a). SdAbs are small (13–15 kDa) targeting molecules derived from the variable regions of heavy chain antibodies from the camelid species (Hamers-Casterman *et al* 1993). In contrast to IgG mAb (150 kDa), sdAbs are one-tenth the size and have low nanomolar affinities when isolated from an immune library (Arbabi Ghahroudi *et al* 1997). In the orthotopic brain tumor model, the tumor grows in its natural environment in the presence of the blood brain barrier (BBB), leading to the formation of a blood tumor barrier (BTB). The BTB can restrict access of exogenous agents to the tumor. Since expression of IGFBP7 is on tumor vessels, rather than on tumor cells, the targeting capability of anti-IGFBP7 sdAb linked to contrast agents can be explored in the more relevant orthotopic brain tumor model without the challenge of traversing the BTB.

In this study, sULVs were used as a nanosized platform for a novel MRI contrast agent by incorporating: PEGylated phospholipid, distearoyl phosphoethanolamine-N-[amino (polyethylene glycol) 2000] (DSPE-PEG2000-Amino) and Gd-DTPA-bis-oleate (Gd-DTPA-BOA). The Gd-sULV contrast agents were linked to the near infrared dye, Cy5.5, and different antibodies, anti-EGFR mAb or anti-IGFBP7 sdAbs, and then imaged using *in vivo* optical imaging in a xenograft (anti-EGFR mAb targeted Gd-sULV) and orthotopic (anti-IGFBP7 sdAb targeted Gd-sULV) brain tumor models in mice. It was found that nanosized sULV loaded with Gd formed spontaneously and can be targeted with antibodies against differentially localized tumor targets, i.e. tumor cells or tumor vessels. In the case of anti-EGFR mAb targeted Gd-sULV, although an improved delivery of contrast agent was evident in the xenograft tumor model, the molecular targeting of EGFR expression was confounded by passive targeting effects. *In vivo* optical imaging and fluorescence microscopy indicated that the anti-IGFBP7 sdAb targeted Gd-sULV showed improved molecular targeting compared to the anti-EGFR mAb targeted Gd-sULV due to the reduced background of the nontargeted Gd-sULV and selective ability to image brain tumor vessels. Finally, the anti-IGFBP7 targeted Gd-sULV was able to image orthotopic brain tumors using MRI.

2. Methods

2.1. Formulation of Gd loaded small unilamellar vesicles (Gd-sULV)

Dimyristoyl phosphatidylglycerol (DMPG), dihexanoyl phosphatidylcholine (DHPC) and distearoyl phosphoethanolamine-N-[amino(polyethylene glycol)2000] (DSPE-PEG2000-

Amino) were purchased from Avanti Polar Lipids (Alabaster, AL, USA). The gadolinium diethylene-triamine-pentaacetic acid bis-oleate (Gd-DTPA-BOA) was custom synthesized (IQSynthesis, Miramar, FL, USA). DMPG/DHPC/DSPE-PEG2000-Amine/Gd-DTPA-BOA at 31, 23.8, 5 and 40 mol%, respectively, were first dissolved in chloroform and dried by continuously flowing N_2 gas, followed by vacuum for 24 h. The dried samples were then re-dispersed in water (D_2O for neutron scattering; H_2O for other tests) to form 10 wt% solutions by temperature cycling and vortexing between 4° and 50 °C (4–5 cycles). The 10 wt% solutions are liquid-like at low T (4 °C), but gel-like at high T (50 °C). All the samples were then diluted with cold D_2O at 4 °C into a total lipid concentration of 2 wt%.

2.2. Dynamic light scattering (DLS) measurements

Dynamic light scattering (DLS) on both nontargeted Gd-sULV and anti-IGFBP7 sdAb-Gd-sULV was performed using a Zetasizer Nano (Malvern Instruments Ltd, Worcestershire, UK). The DLS experiments were carried out at 23 °C on samples dispersed (1:100 v/v) in milli$Q$ water. The size distribution was determined by the intensity-weighted data output.

2.3. Small angle neutron scattering (SANS)

SANS is a technique used to study the structure of a material on the nanoscale level (0.1–100 nm). Information of the size and morphology of particles dispersed in homogeneous mediums can be determined by measuring the scattering of a neutron beam from the sample. In this study, lipid mixtures were dissolved in D_2O of purity >99.9% (Chalk River Laboratories, ON, Canada) to enhance the neutron scattering contrast. All SANS measurements were performed at 50 °C, where the lamellar structure is expected. SANS experiments were conducted at the 30 m NG3 SANS instrument located at the NIST (National Institute of Standards and Technology) Center for Neutron Research (NCNR, Gaithersburg, MD). Six Å wavelength (λ) neutrons and three sample-to-detector distances (i.e., 1, 4 and 13 m) were used, covering a range of scattering vectors ($q = \frac{4\pi}{\lambda}\sin(\frac{\theta}{2})$, θ being the scattering angle) from 0.003 to 0.3 $Å^{-1}$. The raw data were corrected for background (blocked beam) and normalized using the incident neutron beam and sample transmission. Empty cell (water with no sULVs) data, treated in the same manner, were then subtracted. The reduced data were then circularly averaged. The final scattering intensity, I, is a function of scattering vector, q.

2.4. In vitro phantom magnetic resonance imaging (MRI)

The T_1 relaxation properties of samples containing Gd-sULVs were compared to that of Gd-DTPA (Magnevist, Berlex, Canada). Solutions of 50 or 200 μg ml^{-1} Gd concentrations were prepared using Gd-DTPA or Gd-sULVs with either 20 or 40 mol% Gd-DTPA-BOA. These solutions (270 μl) were aliquoted into tubes which were embedded in agarose within a container and scanned using a quadrature coil and a Bruker BioSpec console MRI system with a 9.4 T magnet and Paravision 4 software (Bruker Biospin, Milton, Canada). The T_1 maps of cross-sectional slices through the tubes were acquired using a RARE inversion-recovery sequence with variable repetition times. Three slices were acquired using a matrix of 128 × 128, field of view of 3 cm^2, TE = 10 ms, flip angle of 180° and ten different times of 135, 375, 630, 950, 1300, 1750, 2300, 3100, 4400 and 10 000 ms. The T_1 for each sample was measured from the T_1 maps calculated using the Paravision 4 software (Bruker Biospin, Milton, Canada).

2.5. Cy5.5 labeling of Gd-sULV—a bimodal contrast agent

Gd-sULVs were heated at 55 °C for 30–60 min to promote the formation of spherical Gd-sULVs (Yue *et al* 2005, Nieh *et al* 2005, Mahabir *et al* 2010). The formation of such sULVs is hallmarked by a change in the solution's appearance from opaque to transparent. Once heated, the Gd-sULVs are stable for months at RT and at 4 °C. It should be pointed out that reversion to discoidal micelles is slow (i.e. months) (data not shown). Sodium Bicarbonate buffer (pH 9.3) was added 10% v/v, and 100× molar excess (to the number of estimated Gd-sULVs) of Cy5.5-NHS-ester (GE Healthcare, Buckinghamshire, UK; excitation 670 nm, emission 690 nm) was added and allowed to react for 2 h at RT while mixing. After the incubation period, unbound dye was removed using a 10 kDa Amicon purification column (Millipore, Billerica, MA, USA).

2.6. Cellular internalization of Gd-sULV-Cy5.5

The human glioblastoma parental cell line U87MG and its sublines U87MG.wtEGFR and U87MG.EGFRvIII, which overexpress wild type EGFR and the EGFR type III variant (EGFRvIII), respectively, were kindly provided by Dr W L Cavenee (Ludwig Institute for Cancer Research, La Jolla, CA, USA). Cell lines were cultured and maintained as described previously (Abulrob *et al* 2004). For cellular internalization studies, U87MG.EGFRvIII or U87MG parental cells were plated to confluency on cover slips coated with poly-L-lysine (25 μg ml^{-1}) placed in 24 well plates. The cells were washed twice with warm Dulbecco's modified Eagle's medium (DMEM). The anti-EGFR mAb targeted or nontargeted Gd-sULV-Cy5.5 solution was diluted 1/500 in 300 μl DMEM, and then added to each of the cell lines for 1 h at 37 °C. Cell were then washed five times with ice cold 1X PBS, followed by fixing in 3.7% formaldehyde/PBS solution for 15 min at RT. Excess fixative was washed off with 1X PBS at RT. Fixed cells were incubated for 1 min with 1:500 WGA-FITC/PBS on ice, washed with 1X PBS three times, and then mounted on slides using DAKO mounting medium containing 1 μg ml^{-1} Hoechst. Cells were then visualized under an Olympus 1× 81 inverted motorized microscopes (Olympus, Markham, ON, Canada). *In vivo* and ImagePro 6.2 software (Olympus, Markham, ON, Canada) were used to acquire and analyze images.

2.7. Pharmacokinetics

Two hundred microlitres of a Cy5.5 labeled Gd-sULVs solution (2% w/v) were injected via the tail vein in normal CD-1

mice. Fifty microlitres volume blood samples were collected in heparinized tubes by creating a small nick in the tail vein. Collection was carried out over a period of 24 h (i.e., 5 min, 30 min, 1 h, 1.5 h, 2 h, 4 h and 24 h). Samples were then analyzed for Cy5.5 labeled Gd-sULVs using a fluorescent plate reader with an excitation wavelength of 670 nm and an emission wavelength of 690 nm, and quantified using a standard curve of known Cy5.5 labeled sULV concentrations in whole blood. Pharmacokinetic parameters were calculated using the 5.2 version WinNonlin software package (Pharsight Corporation, Mountain View CA, USA). A two-compartment IV-Bolus model was selected for pharmacokinetic modeling, as it best represented the actual data. This model is described by the following equation: $C(t) = A\exp(-\alpha t) + B\exp(-\beta t)$, where $C(t)$ represents the agent's concentration in serum. A and B represent the zero time intercept of the alpha phase and beta phase, respectively, α and β are disposition rate constants, and $\alpha > \beta$. The area under the serum concentration–time curve was calculated with the equation $AUC_{0-\infty} = D/V/K_{10}$, where D is the dose given, V is the apparent distribution volume and K_{10} is the elimination rate constant. Total clearance was determined from the equation $Cl/F = D/AUC_{0-\infty}$.

2.8. Production of anti-IGFBP7 sdAb

Isolation of anti-IGFBP7 sdAbs were achieved by llama immunization with recombinant human IGFBP7 protein (Pen *et al* 2008) and the construction of an immune phage display library. Subsequent panning and selection was undertaken as previously described (Iqbal *et al* 2010a).

2.9. Bioconjugation of anti-EGFR mAb or anti-IGFBP7 sdAb to Gd-sULV-Cy5.5

The anti-EGFR mAb (1 mg) or anti-IGFBP7 sdAb (1 mg) was resuspended in MES buffer (0.1 M MES, 0.5 M NaCl, pH 5.5). Sulfo-NHS and EDC in MES buffer were added to each antibody solution to a final concentration of 10 mM and 4 mM, respectively. The reaction tube was flushed with N_2 gas and reacted at RT for 30 min with mixing. The reaction was quenched by the addition of hydroxylamine HCl to a final concentration of 5 mM. The antibodies were purified in MES buffer using 10 K Amicon columns (Millipore, Billerica, MA, USA). One ml of Gd-sULVs-Cy5.5 (2% w/v solution) in 10% sodium bicarbonate buffer were added to the antibody solution and reacted at RT for 4–6 h while mixing.

2.10. Xenograft and intracranial models of U87MG.EGFRvIII glioblastoma in nude mice

All animal procedures were approved by the NRC-IBS or NRC-IBD (West) Animal Care Committee and were in compliance with the Canadian Council of Animal Care. CD-1 nude mice (males, 6–8 weeks old) were purchased from Charles River Canada. The animals were housed in cages in groups of 4, maintained on a 12 h light/dark schedule at a temperature of 22 °C and a relative humidity of 50 ± 5%. Food and water was available *ad libitum*. U87MG.EGFRvIII carrying the deletion mutant of EGFR (EGFRvIII) cells was cultured in DMEM supplemented with 10% fetal calf serum and maintained in a humidified 5% CO_2 atmosphere at 37 °C. This EGFRvIII mutation confers enhanced tumorgenicity *in vivo* (Nagane *et al* 1996) and there is differential expression of the EGFR protein compared to the U87MG parental cell line (Zhang *et al* 2003). Cells were harvested by trypsinization in EDTA/trypsin, washed in PBS, and centrifuged three times at 200 g for 2 min. Cell number was determined and mice were injected subcutaneously in the left foreleg with 2×10^6 U87MG.EGFRvIII glioblastoma cells suspended in 100 μl of phosphate-buffered saline (PBS). Xenograft tumor bearing mice were subjected to *in vivo* imaging studies when the tumors reached 0.4 cm in diameter (14 d after implant).

For intracerebral implantation of U87MG.EGFRvIII cells, mice were anesthetized with isofluorane anesthesia and the scalp was swabbed with alcohol. The skin was incised and a 10 μl Hamilton syringe was used to inoculate a 2 μl cell suspension (50 000 cells) into the corpus striatum in the left hemisphere (3.0 mm deep; 1 mm anterior and 2.0 mm lateral to the bregma). The U87MG.EGFRvIII implanted tumors were allowed to grow for 10 days before the beginning of imaging experiments.

2.11. In vivo near-infrared fluorescence imaging of antibody targeted Gd-sULVs in brain tumors

Mice bearing 14 day old U87MG.EGFRvIII xenograft brain tumors were injected with anti-EGFR mAb targeted Gd-sULV-Cy5.5 or nontargeted Gd-sULV-Cy5.5 via the tail vein (0.2 mls of 2% wt solution). In another set of animals, mice bearing ten day old U87MG.EGFRvIII intracranial brain tumors were injected with anti-IGFBP7 sdAb targeted Gd-sULV-Cy5.5 or nontargeted Gd-sULV-Cy5.5 via the tail vein (0.2 mls of 2% wt solution). Animals were subjected to *in vivo* imaging studies using a small-animal time-domain eXplore Optix MX2 pre-clinical imager (Advanced Research Technologies, Montreal, QC, Canada), as described previously (Abulrob *et al* 2007, 2008, Iqbal *et al* 2010b). In all imaging experiments, a 670 nm pulsed laser diode was used for excitation, and the fluorescence emission was collected at 700 nm. Each animal was imaged dorsally in the head region and whole body at various time points after i.v. injection. The data were recorded as temporal point-spread functions (TPSF) and the images were reconstructed as fluorescence concentration maps. Average fluorescence concentration data from ROIs placed around the tumor region, or contralateral muscle (for xenograft tumor analysis only), were subsequently analyzed using the OptiView software package (Advanced Research Technologies, Montreal, QC, Canada). At the end of the experiment mice bearing intracranial U87MG.EGFRvIII brain tumors were i.v. injected with 40 μg of fluorescein labeled tomato lectin 10 min prior to being sacrificed, in order to stain the brain vessels. All animals were then perfused with heparinized saline and organs were excised and imaged *ex vivo*. *Ex vivo* organs were analyzed by placing an ROI around each organ and determining the total fluorescence concentration per gram tissue.

2.12. Fluorescent microscopy

Organs and tumor tissue were frozen on dry ice and stored at −80 °C. For xenograft tumors, tumor tissues were embedded in Tissue-Tek freezing medium (Miles Laboratories, Elkhart, IN) and sectioned on a cryostat (Jung CM3000; Leica, Richmond Hill, ON, Canada) in 10 μm thick slices, then mounted on Superfrost Plus microscope slides (Fisher Scientific, Nepean, ON, Canada). Slides were stored at −80 °C until immunohistochemical studies. Frozen xenograft brain tumor sections were thawed for a few seconds then incubated in methanol for 10 min at room temperature. Slides were rinsed with 0.2 M PBS (pH 7.3), followed by incubation with 5% goat serum in PBS for 1 h with 0.1% triton-X 100 at room temperature. After blocking, slides were incubated with the anti-epidermal growth factor receptor (EGFR) antibody as a tumor biomarker, and then visualized using the goat anti-rabbit alexa 488 secondary antibody. Slides were then washed five times with PBS and dried of excess liquid. The coverslips were then mounted using DAKO fluorescent mounting media. Coverslips were allowed to harden at 4 °C overnight and then visualized under a fluorescent microscope. For mouse brains containing intracranial tumors, brains were fixed in paraformaldehyde for 24 h, after which coronal sections (50 μm) were produced using a Vibratome sectioning instrument (Ted Pella, Redding, CA, USA). Tissue sections were stored at 4 °C in low molarity PBS with 0.1% NaN_3. Tissue sections were mounted on Superfrost Plus microscope slides using mounting media containing 2 μg ml^{-1} of Hoescht nuclei stain (Sigma). All sections were then visualized under an Olympus 1× 81 inverted motorized microscope (Olympus, Markham, ON, Canada). InVivo and ImagePro 6.2 software (Olympus, Markham, ON, Canada) were used to acquire and analyze images.

2.13. Determination of total Gd in tumor and muscle tissues using inductively coupled plasma mass spectrometry (ICP-MS)

The ICP-MS instrument was an ELAN 6000 (PerkinElmer SCIEX, Thornhill, ON, Canada). The digested tumor or muscle samples were introduced into the ICP via a cross-flow nebulizer fitted in a Ryton spray chamber. Nitric acid was purified in-house prior to use by sub-boiling distillation of reagent-grade feedstock in a quartz still. High-purity de-ionized water (DIW) was obtained from a NanoPure mixed bed ion-exchange system fed with reverse osmosis domestic feed water (Barnstead/Thermolyne Corp, Iowa, USA).

Samples up to 50 mg of the freeze dried tumor, or muscle tissue, were digested in a PTFE vessel heated at 90 °C for 6 h with 500 μl nitric acid (69%) containing rhodium (10 μg l^{-1}) as an internal standard. The clear solution was diluted 15 times and analyzed with ICP-MS. Concentrations of Gd were determined by external calibration using values obtained after rhodium normalization.

2.14. In vivo MRI of anti-IGFBP7 sdAb targeted and nontargeted Gd-sULVs

Tumor cells were implanted into CD-1 nude mice brains as described above. Seven to eight days following intracranial implantation animals were scanned using standard T2 imaging (see below) to confirm successful tumor implantation. Ten days following injection, animals were anesthetized with isoflurane for contrast imaging using MRI. First, the femoral vein was isolated and a catheter was inserted into the vein for contrast administration. The mouse was then moved into a cradle for positioning into the center of a 9.4 T magnet equipped for MRI using a Bruker BioSpec console. Animals were randomized into targeted and nontargeted contrast injection groups.

In general, prior to contrast injection, T2 weighted, T1 weighted and in later animals, T1 maps were acquired using a 2 × 2 cm^2 field of view and a 128 × 128 data matrix. The T2 weighted scans for anatomical imaging consisted of acquiring ten 1.0 mm thick slices centered at the level of the striatum using a RARE sequence with a repetition time of 5000 ms and an echo time of 60 ms. The T_1 weighted images (10 slices) were acquired with a RARE sequence using a repetition time of 750 ms, an echo time of 7.56 ms and 7 averages. The T_1 maps were acquired using a single shot echo planar sequence with a repetition time of 8.5 s, an echo time of 38 ms and 22 inversion time points every 400 ms for a 1 mm thick slice through the tumor. The T1 values in the tumor and brain were measured using the Bruker Avance II software. After the pre-injection scans, either targeted or nontargeted contrast were injected intravenously (0.20 ml of 2% w/v Gd-sULV solution) and MR imaging was repeated at 2 h post-injection. The effect of contrast was assessed using differences in intensity in the T1 weighted images by subtracting the pre-T1 weighted images from the final T1 weighted images.

2.15. Statistical analysis

All data are reported as mean ± SEM, and the differences between groups were determined using two-way ANOVA followed by the Bonferoni post hoc test. Differences greater than $P < 0.05$ were considered significant.

3. Results

3.1. Characterization of Gd-sULV

To study the stability of the resultant structure of nontargeted Gd-sULV as a function of annealing time, SANS measurements on both 0.5 and 1.0 wt% samples incubated at 50 °C for either 18 h or three days, were conducted. SANS data (figure 1(B)) of both samples showed no smectic peaks associated with multi-lamellar vesicles, which otherwise would form in Gd-DTPA-BOA aqueous solutions (figure 1(B)).

An oblate shell model (schematic shown in figure 1(A)) was applied to fit the SANS data. This model includes four structural parameters: (a) the long core axis (a_{core}); (b) the short core axis (b_{core}); (c) shell thickness (t); (d) the polydispersity of b_{core}. The equation $P(q)$ describing the model can be expressed as follows.

$$P(q) = \int_0^{\pi/2} \partial V_{\text{T}} \left[\frac{(\rho_{\text{core}} - \rho_{\text{shell}}) U(u_{\text{core}}) V\text{core}}{u_{\text{core}} V_{\text{T}}} + \frac{(\rho_{\text{D}_2\text{O}} - \rho_{\text{shell}}) U(u_{\text{shell}})}{u_{\text{shell}}} \right]^2 \sin\theta \, \mathrm{d}\theta$$

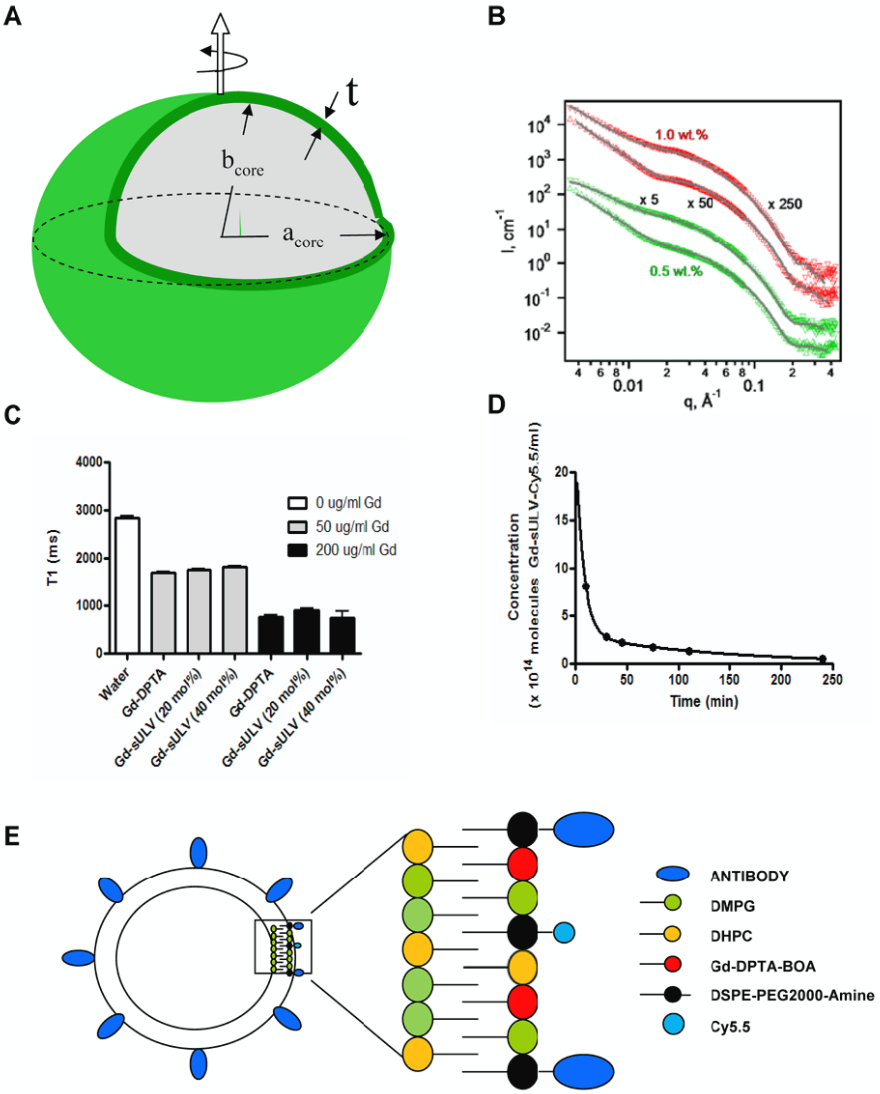

Figure 1. Small unilamellar vesicles (ULVs) with high Gd payload. (A) Schematic of the ellipsoidal shell model of sULVs. This model includes four structural parameters: (a) long core axis (a_{core}); (b) short core axis (b_{core}); (c) shell thickness (t); (d) the polydispersity of b_{core}. (B) Small angle neutron scattering (SANS) of a 40 mol% Gd-sULVs mixture with total lipid concentrations of 0.5 (green) and 1.0 (red) wt% annealed at 50 °C for 18 h (inverted triangles) and 3 days (triangles). (C) The *in vitro* T1 relaxation of 20 mol% and 40 mol% Gd-sULV samples was compared to Gd-DPTA solutions at 0, 50 or 200 μg ml^{-1} Gd concentrations. (D) Pharmacokinetic profile indicating the concentration in blood over time of the Gd-sULV-Cy5.5 after intravenous injection. (E) Schematic diagram of the antibody targeted Gd-sULV-Cy5.5 with its various lipid components. DMPG, dimyristoyl phosphatidylglycerol (DMPG). DHPC, dihexanoyl phosphatidylcholine, Gd-DPTA-BOA, gadolinium diethylene-triamine-pentaacetic acid bis-oleate, DSPE-PEG2000-Amine, distearoyl phosphoethanolamine-N-[amino (polyethylene glycol) 2000].

(This figure is in colour only in the electronic version)

where the particle orientation function $U(x)$ can be written as

$$U(x) = \frac{(\sin x - x\cos x)}{x^2}$$

and

$$u_{\text{core}} = q[a_{\text{core}}^2 \sin^2\theta + b_{\text{core}}^2 \cos^2\theta],$$

$$u_{\text{core}} = q[(a_{\text{core}} + t)^2 \sin^2\theta + (b_{\text{core}} + t)^2 \cos^2\theta].$$

V_{T} and V_{core} represent the total volume of the oblate vesicle (i.e., $\frac{4\pi}{3}[(a_{\text{core}} + t)^2(b_{\text{core}} + t)]$) and the core volume (presumably entrapped water) of vesicle (i.e., $\frac{4\pi}{3}a_{\text{core}}^2 b_{\text{core}}$), respectively. Polydispersity of b_{core} (the most sensitive structural parameter in this q range) is also incorporated into the equation, which is then integrated using the Gaussian–Laguerre integration method.

All the best fits agree well with the experimental data, and the best-fitted values of the parameters are listed in table 1. Although the SANS data show significant differences in the low-q regime, the structural parameters obtained from the fits to the data do not differ dramatically, with the exception of a_{core}, which is greater in the 1.0 wt% sample. The best-fit

Table 1. Best-fit ellipsoidal shell model data for Gd-sULV samples at 50 °C for 18 h and 3 days.

	0.5 wt%		1.0 wt%	
	18 h	3 days	18 h	3 days
a_{core} (Å)	625	570	1070	1230
b_{core} (Å)	65	59	60	64
t (Å)	38	38	39	38
Polydispersity	0.48	0.5	0.49	0.46
$(r_{core} - r_{shell})$ (Å^{-2})	6.6×10^{-6}	6.2×10^{-6}	6.7×10^{-6}	6.0×10^{-6}
$(r_{D2O} - r_{shell})$ (Å^{-2})	4.1×10^{-6}	4.6×10^{-6}	4.2×10^{-6}	4.7×10^{-6}

results of 18 h and three days (0.5 wt% and 1 wt% samples) data show that they differ in contrast, the difference of neutron scattering length densities between core and shell as well as D_2O and core ($(\rho_{core} - \rho_{shell})$ and $(\rho_{core} - \rho_{shell})$ in table 1). Such a difference in contrast between the two samples may be the result of the PEG chains rearranging at high temperature. However, the reason for the higher value of the best-fit result for the scattering length density of the nanoparticle core, ρ_{core}, compared to that of D_2O, ρ_{D2O}, is not presently understood.

DLS of the nontargeted Gd-sULV revealed a hydrodynamic diameter of 30 nm. These values seem to underestimate the dimension of the Gd-sULV, however, it lies in between $2(a_{core} + t)$ and $2(b_{core} + t)$ obtained from SANS data. DLS result of the Gd-sULV bioconjugated with sdAb indicates an average particle size of 41 nm, slightly increased from the nontargeted Gd-sULVs due to the addition of conjugated sdAb and implying that the structure of Gd-sULVs remains intact.

3.2. Effects of Gd-sULVs on in vitro phantom T_1 relaxation

The T_1 signals of samples containing either Gd-DTPA or Gd-sULVs were similar when the concentration of total Gd within the sample was similar. The T_1 of samples containing 50 or 200 μg ml^{-1} of Gd were similar irrespective of whether the Gd was free or within the vesicles (figure 1(C)). Since each vesicle contained a high payload of Gd, in order to obtain a similar T_1 effect for the 40 mol% Gd-sULV, approximately 10 times more of 20 mol% Gd-sULVs and approximately 5540 times more Gd-DTPA molecules were required. According to the observed T1 effects, relaxivity of Gd-DTPA in water at 9.4 T was 4.45 ± 0.24 mM^{-1} s^{-1} compared to 3.80 ± 0.31 mM^{-1} s^{-1} and 4.30 ± 0.95 mM^{-1} s^{-1} for the 20 mol% and 40 mol% solutions, respectively—these values were calculated according to the total Gd concentration in the samples. If relaxivity was considered according to the molar concentration of particles, the contrast solutions had a T_1 relaxivity of 2220 ± 280 and $23\,800 \pm 5270$ mM^{-1} s^{-1} for the 20 mol% and 40 mol% solutions, respectively.

3.3. Cellular internalization of anti-EGFR mAb targeted or nontargeted Gd-sULV-Cy5.5 in U87MG.EGFRvIII or U87MG parental cell lines in vitro

Incubation of anti-EGFR mAb targeted Gd-sULVs-Cy5.5 for 1 h with U87MG.EGFRvIII cells (figure 2, upper left panel), but not U87MG parental cells (which have little or no detectable EGFR receptors, Iqbal *et al* 2010b) (figure 2, upper right panel), resulted in widespread cellular uptake into the cell cytoplasm with well-defined punctuate intensities, presumably representing sULVs entrapped in endosomal compartments. In comparison, Gd-sULVs-Cy5.5 incubated with either the U87MG.EGFRvIII (figure 2, lower left panel) or U87MG parental (figure 2, lower right panel) cell line demonstrated reduced internalization in comparison to the anti-EGFR mAb targeted Gd-sULVs-Cy5.5. These results suggest that anti-EGFR mAb targeting can facilitate active targeting in cells that overexpress the EGFR receptor.

3.4. Pharmacokinetic analysis of Gd-sULV-Cy5.5 in vivo

In vivo pharmacokinetic analysis of Gd-sULV's injected intravenously via the mouse tail, followed by repeated blood sampling, indicated a half-life of 1.67 h and an apparent volume of distribution (Vss) of 2.8 ml. Therefore, the PK parameters of the Gd-sULV indicate a full clearance of the nanoparticles within 8 h (∼5 half-lives).

3.5. Anti-EGFR mAb targeted Gd-sULV-Cy5.5 in U87MG.EGFRvIII xenograft model in mice

The xenograft brain tumor model in mice was chosen to evaluate the targeting ability of anti-EGFR mAb targeted Gd-sULV-Cy5.5, as it allows for the extravasation of circulating agents past the tumor vessels, with a porous BTB. To examine targeting, the biodistribution of anti-EGFR mAb-Gd-sULVs-Cy5.5 and nontargeted Gd-sULVs-Cy5.5 was determined by *in vivo* optical imaging in mice bearing 14 day old xenograft GBM tumors. A peak in the optical signal was observed approximately 8 h post-injection for anti-EGFR mAb targeted Gd-sULVs (figure 3(A)). The peak signal in the tumor appeared to be stable at 24 h, at which point a statistically significant difference was demonstrated (figure 3(C)).

Anti-EGFR mAb targeted formulations achieved a higher tumor to muscle ratio of 2.7 compared to nontargeted formulations, which had a ratio of 1.6. Tumor to muscle ratio was determined by dividing the average fluorescence concentration in the tumor region to that of the contralateral muscle using a similarly sized ROI.

Ex vivo, the extracted tumor tissue for anti-EGFR mAb targeted Gd-sULVs was approximately 80% higher in average fluorescence concentration than the nontargeted Gd-sULVs (figure 3(A)). Fluorescence from contralateral muscle tissue for both anti-EGFR mAb and nontargeted Gd-sULVs was similar. ICP-MS analysis of Gd content in the extracted tumors and

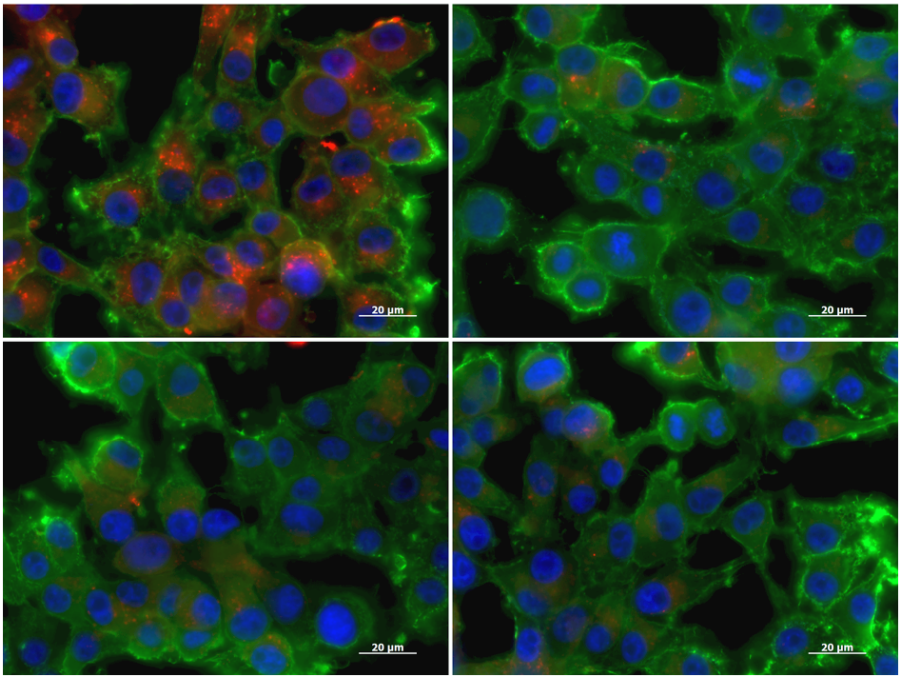

Figure 2. Anti-EGFR mAb targeted Gd-sULVs demonstrate internalization in U87MG.EGFRvIII cancer cells *in vitro*. Representative immunofluorescence images of either anti-EGFR mAb targeted (left panels) or nontargeted (right panels) Gd-sULVs-Cy5.5 incubated with either U87MG.EGFRvIII (upper panels) or U87MG parental (lower panels) cells for 1 h at 37 °C in 24-well plates. Targeted or nontargeted Gd-sULV-Cy5.5 are shown in red, cell nuclei in blue and cell membrane in green. Scale bar: 20 μm.

contralateral muscles also demonstrated an 80% increase in Gd delivery for the anti-EGFR mAb, compared to the nontargeted Gd-sULVs (figure 3(B)). These ICP-MS results corroborate well with the *ex vivo* optical imaging data.

Sections from xenograft GBM tumor-bearing mice receiving anti-EGFR mAb-Gd-sULVs-Cy5.5 demonstrated stronger Cy5.5 fluorescence (red) in the tumor region, compared to nontargeted Gd-sULVs-Cy5.5 (figure 3(D)). The cellular locations of the anti-EGFR mAb targeted Gd-sULVs-Cy5.5 demonstrated increased internalization within U87MG.EGFRvIII cells compared to the nontargeted Gd-sULV-Cy5.5.

3.6. Anti-IGFBP7 sdAb targeted Gd-sULV-Cy5.5 in an orthotopic U87MG brain tumor model in mice

To examine the targeting ability of anti-IGFBP7 sdAb targeted Gd-sULV-Cy5.5, the more relevant orthotopic brain tumor model was used, which possesses a BTB that restricts access to exogenous agents and an overexpression of the IGFBP7 target in tumor vessels. Targeting vessels, rather than tumor cells, avoids the requirement of bypassing the BTB. *In vivo* biodistribution of the systemically injected anti-IGFBP7 sdAb-Gd-ULV-Cy5.5 was compared with nontargeted Gd-sULV-Cy5.5 in mice bearing 10 day old U87MG.EGFRvIII orthotopic GBM tumors using *in vivo* optical imaging of the head (figure 4(A)). The anti-IGFBP7 sdAb-Gd-sULV-Cy5.5 targeted to brain tumor vessels with a peak signal at 2–4 h (figure 4(B)). Nontargeted Gd-sULVs-Cy5.5 demonstrated very little accumulation. A full body dorsal scan of the GBM bearing mice at 4 h demonstrated that tumor localization of anti-IGFBP7 sdAb targeted Gd-sULVs-Cy5.5 was a prominent signal in the body (figure 4(C)). It was apparent from the full body dorsal scan at 4 h that the concentration in nonspecific areas (i.e. areas without major organs) was similar between the nontargeted and anti-IGFBP7 sdAb targeted Gd-sULV-Cy5.5. This result suggests that the bioconjugation of sdAb to the Gd-sULV did not grossly affect the pharmacokinetics compared to the nontargeted Gd-sULV. At 24 h the anti-IGFBP7 sdAb-Gd-sULV-Cy5.5 formulation was cleared to a similar level to that of nontargeted Gd-sULV-Cy5.5 in the tumor region of the mice (figure 4(B)).

Ex vivo optical imaging at 4 h comparing the biodistribution of the anti-IGFBP7 sdAb targeted Gd-sULV-Cy5.5 to the nontargeted Gd-ULV-Cy5.5 indicated a distinct signal from the brain tumor region (figure 5(A)). There was a higher signal from the brain tumor for the anti-IGFBP7 sdAb targeted Gd-sULV-Cy5.5 group compared to the nontargeted Gd-sULV-Cy5.5 group (figure 5(B)). The highest optical signals originated from the liver for both targeted and nontargeted Gd-sULV-Cy5.5, which is the major route for metabolism for Gd-sULV-Cy5.5. The signal in the kidneys is due to the release of free Cy5.5 after metabolism/degradation in the body.

At the peak imaging signal (4 h after injection), brain sections were analyzed by fluorescent microscopy to examine localization of injected anti-IGFBP7 sdAb-Gd-sULV-Cy5.5 (figure 5(C), left panel) and nontargeted Gd-ULV-Cy5.5 (figure 5(C), right panel). *In vivo* injected tomato lectin-FITC has been previously used to stain brain vascular networks in mice (Iqbal *et al* 2010b, 2010a). In this study, brain tumor vessels were co-stained with tomato lectin and anti-IGFBP7 sdAb-Gd-sULV-Cy5.5 fluorescence, while non

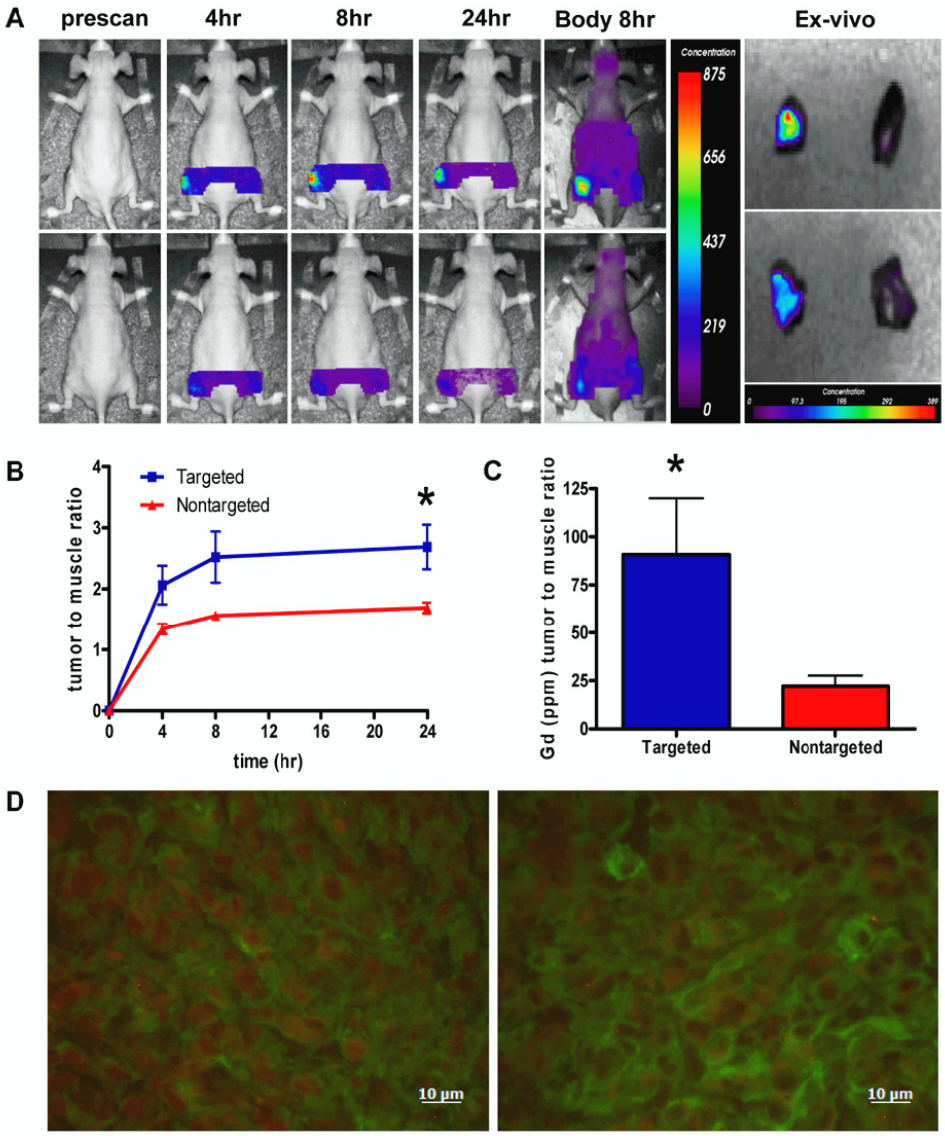

Figure 3. Enhanced accumulation and retention of anti-EGFR mAb targeted Gd-sULV-Cy5.5 in a subcutaneous xenograft tumor model. EGFR mAb targeted and nontargeted Gd-sULV-Cy5.5 were injected intravenously into nude mice bearing 14 day old U87MG.EGFRvIII subcutaneous tumors in their left flank. (A) Mice were subjected to *in vivo* and *ex vivo* fluorescent imaging using the small-animal, time-domain eXplore Optix MX2 pre-clinical imager over 24 h. (B) Total Gd content per mg tissue in the tumor or contralateral muscle, as determined from ICP-MS, was expressed as a tumor to muscle ratio, and then plotted. (C) Raw fluorescence *in vivo* image data from the tumor and contralateral flank region for targeted and nontargeted experiments were also plotted as a function of time. Values correspond to mean ± SEM, $n = 5$–6 per group. * denotes a statistically significant difference ($p < 0.05$). (D) Representative fluorescent microscopy images of 50 μm tumor sections from EGFR mAb targeted (left panel) or nontargeted (right panel) Gd-sULV-Cy5.5 (red signal). The EGFR expression is shown in green.

tomato lectin stained healthy brain tissue vessels did not show the presence of the injected anti-IGFBP7 sdAb-Gd-sULV-Cy5.5. In nontargeted Gd-ULV-Cy5.5 tumor sections, Cy5.5 fluorescence was not apparent.

3.7. MRI of anti-IGFBP7 sdAb targeted Gd-sULV-Cy5.5 in the orthotopic U87MG.EGFRvIII brain tumor model in mice

In vivo optical imaging revealed that anti-IGFBP7 sdAb targeted Gd-sULV-Cy5.5 exhibited more active targeting with little passive targeting (i.e. background). As a result, the anti-IGFBP7 sdAb targeted Gd-sULV-Cy5.5 was selected to be tested further using *in vivo* MRI. Differences in intensity related to contrast accumulation or retention in the tissue were apparent in T1 weighted MRI images obtained at 9.4 T. Images were acquired following injection of either anti-IGFBP7 sdAb-Gd-sULV (e.g. figure 6(A), upper panel) or nontargeted Gd-ULV (e.g. figure 6(A), lower panel). In general, prior to contrast injection, the tumor was poorly visible in the T1 weighted scans. The distinction between brain and tumor became more evident after injection with the Gd-sULV labeled with anti-IGFBP7, but not the nontargeted Gd-sULV. A composite image obtained by subtracting the MRI scan obtained at 2 h post-injection from that prior to injection

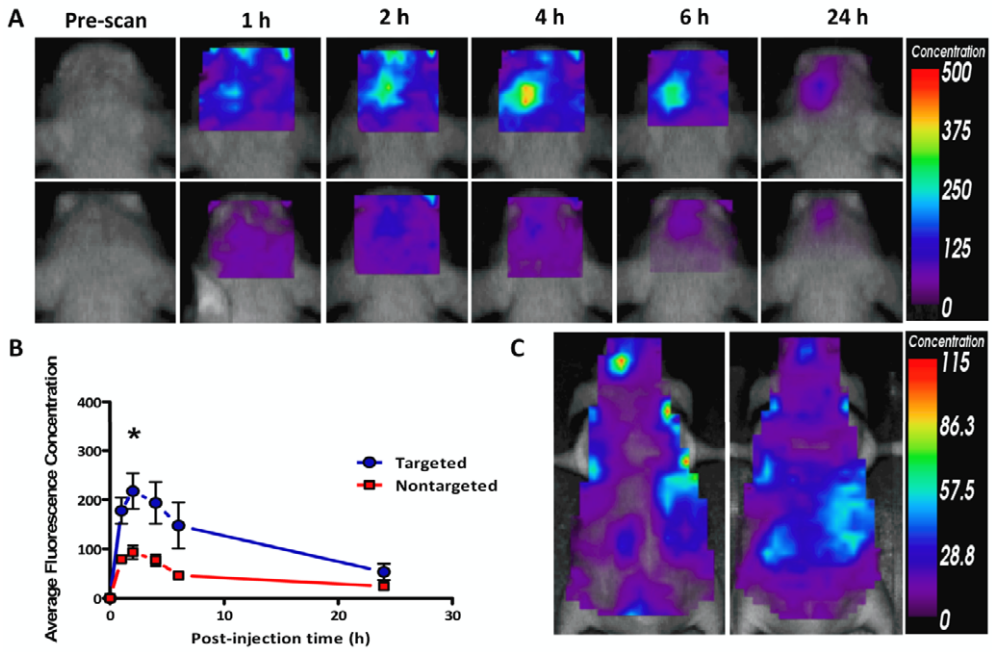

Figure 4. Enhanced targeting of anti-IGFBP7 sdAb targeted Gd-sULVs in an orthotopic brain tumor model. *In vivo* optical imaging of the biodistribution of nontargeted and anti-IGFBP7 sdAb targeted Gd-sULVs-Cy5.5 injected in mice bearing orthotopic glioblastoma tumors. (A) Prospective *in vivo* images of the head at various time points after intravenous injection of anti-IGFBP7 targeted (upper panels) and nontargeted (lower panels) Gd-sULVs-Cy5.5. (B) Graph showing changes of the average fluorescence concentration in the brain tumor region *in vivo* at indicated times after the injection of either anti-IGFBP7 sdAb targeted or nontargeted Gd-sULVs-Cy5.5. Data are expressed as mean ± SEM for $n = 5$ animals. * indicates significant difference between anti-IGFBP7 sdAb targeted Gd-sULV-Cy5.5 and nontargeted Gd-sULV-Cy5.5 ($P < 0.01$). (C) *In vivo* optical images of a whole animal body at 24 h after injection of anti-IGFBP7 targeted (left panel) and nontargeted (right panel) Gd-sULV-Cy5.5.

directly illustrates the contrast enhanced areas due to the accumulation or retention of anti-IGFBP7 sdAb targeted Gd-sULV (figure 6(A), right panels). Quantitative measurement of intensities in T1 weighted images for regions of tumor and comparable contralateral areas of normal brain (figure 6(B)), confirm an increased contrast between brain and tumor at 2 h following injection of the anti-IGFBP7 sdAb labeled ULVs ($p < 0.001$), but not in the case of the nontargeted ULVs. A similar trend was observed, with the differences in T_1 values between tumor and brain being a mean of 119 ± 11.0 ms and 59.7 + 11.8 ms, following targeted or nontargeted contrast injection, respectively.

4. Discussion

Improving MRI detection of disease processes by using contrast agents is a major goal of the molecular MRI community. This sensitivity can be improved by either delivering more Gd and/or increasing the targeting of the Gd to the site of interest, where selection of the appropriate target is a critical factor. In this study, efforts were made to do all of the above. To improve on the design of Gd loaded liposomes (which are traditionally produced by laborious filtration methods), a process for formulating stable, self-assembled monodisperse and nanosized sULVs loaded with Gd was developed. These spontaneously forming sULVs have advantages over liposomes in their scalability of manufacturing, their size, and favorable pharmacokinetics for molecular imaging applications.

To increase target specificity of Gd-sULVs, a suitable molecular target is required that is abundant, accessible and specific for the disease. In this study, the IGFBP7 (tumor vessel specific), and the EGFR (tumor cell specific) targets meet these requirements for the orthotopic and xenograft brain tumor models, respectively. Both of these targets are highly expressed in brain tumors, but differ in their cellular location, i.e. tumor vessels versus tumor cells. To target EGFR, an anti-EGFR mAb was utilized. Although monoclonal antibodies can target contrast imaging agent carriers to the antigen recognition site, these antibodies are relatively large (150 kDa) proteins, and can only be attached to nanoparticles in low numbers. In this study, it was estimated that 1–2 mAbs per Gd-sULV were successfully bioconjugated. Since a large number of mAb could not be incorporated onto the sULVs, the possibility of increased avidity effects through polyvalency is limited (Tassa *et al* 2010). Moreover, repetitive display of large proteins on the surface of nanoparticles can be immunogenic, and in some instances accelerate biological clearance (Drummond *et al* 2008). This is due to the recognition of the Fc portion of the mAb by macrophages. In comparison, to target the IGFBP7 localized in tumor vessels, an anti-IGFBP7 sdAb was utilized. For the sdAb, it was estimated that approximately 10 sdAbs per Gd-sULV were bioconjugated. The use of antibody fragments such as single domain or single chain

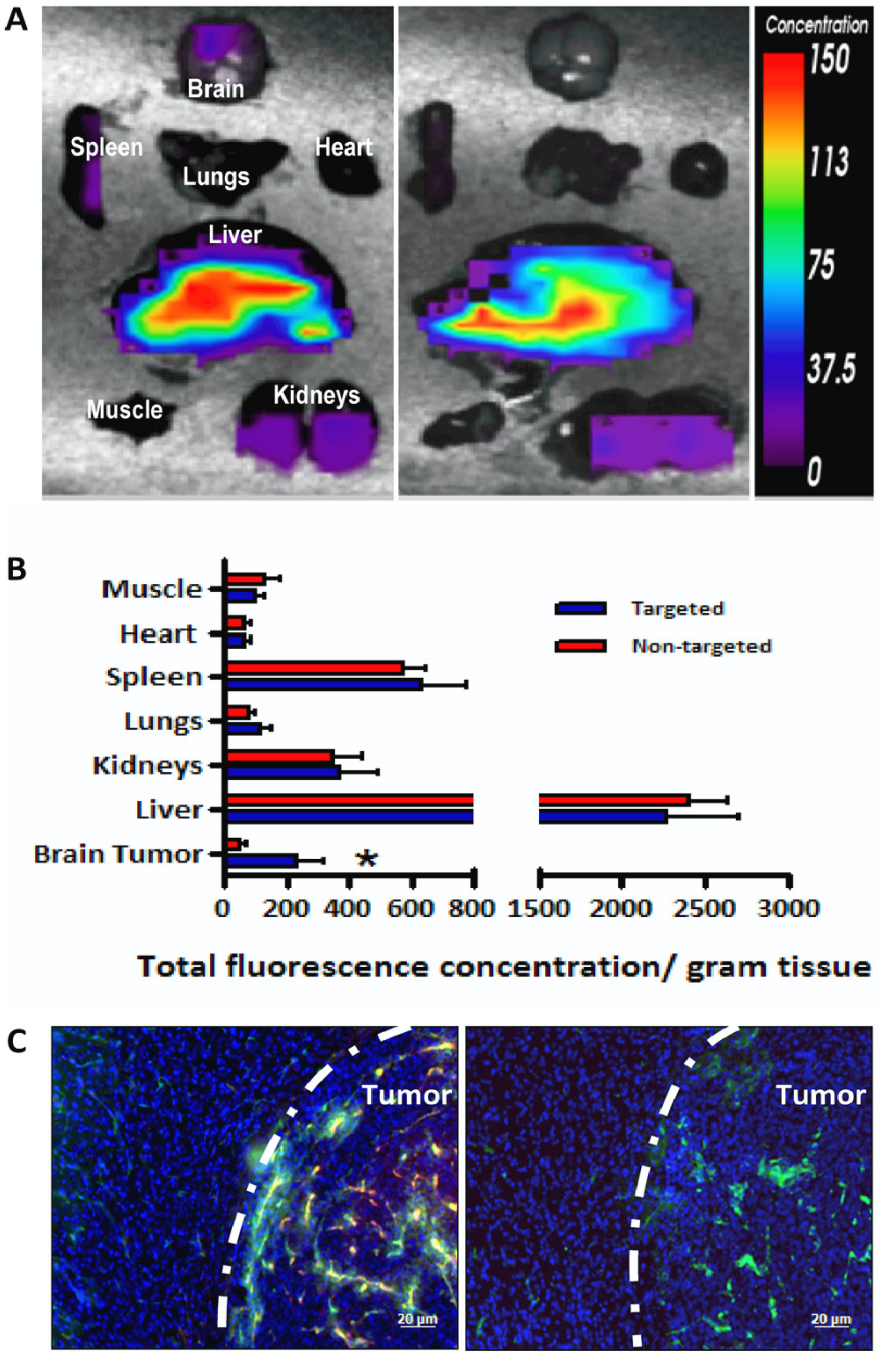

Figure 5. Biodistribution of anti-IGFBP7 sdAb targeted Gd-sULV-Cy5.5 in *ex vivo* organs. (A) *Ex vivo* optical imaging of the organ biodistribution of anti-IGFBP7 sdAb targeted (left panel) and nontargeted (right panel) Gd-sULVs-Cy5.5 24 h after injection in mice bearing orthotopic glioblastoma tumors. (B) Graph illustrating the total fluorescence concentration per gram tissue in organs imaged *ex vivo* 4 h after the injection of either anti-IGFBP7 sdAb targeted or nontargeted Gd-sULV-Cy5.5. (C) Fluorescent microscopic images of mouse GBM tumor sections obtained 4 h after intravenous injection of anti-IGFBP7 sdAb targeted (left panel) or nontargeted (right panel) Gd-sULVs-Cy5.5 (red). Mice were also injected with 40 μg of FITC labeled tomato lectin, 10 min before sacrifice, to stain blood vessels *in vivo*. Lectin staining (green) co-localizes with the Gd-sULV-Cy5.5 signal (red) in overlay images. Cell nuclei are stained with DAPI (blue). Scale bar: 50 μm.

antibodies are not expected to affect the half-life of the Gd-sULV, nor increase liposomal uptake by macrophages, since they do not possess an Fc portion (Sapra *et al* 2004, Roopenian and Akilesh 2007). Furthermore, sdAbs are more easily produced and soluble compared to conventional antibodies, an important consideration in regards to the scalability of a system (Arbabi Ghahroudi *et al* 1997). Alternatively, peptides can also be used as targeting moieties, but often suffer from low affinity/specificity and are prone to degradation by proteases (Sulochana and Ge 2007). A more objective study comparing the targeting ability of mAb and sdAb against the same tumor target is warranted in the future. Despite these differences,

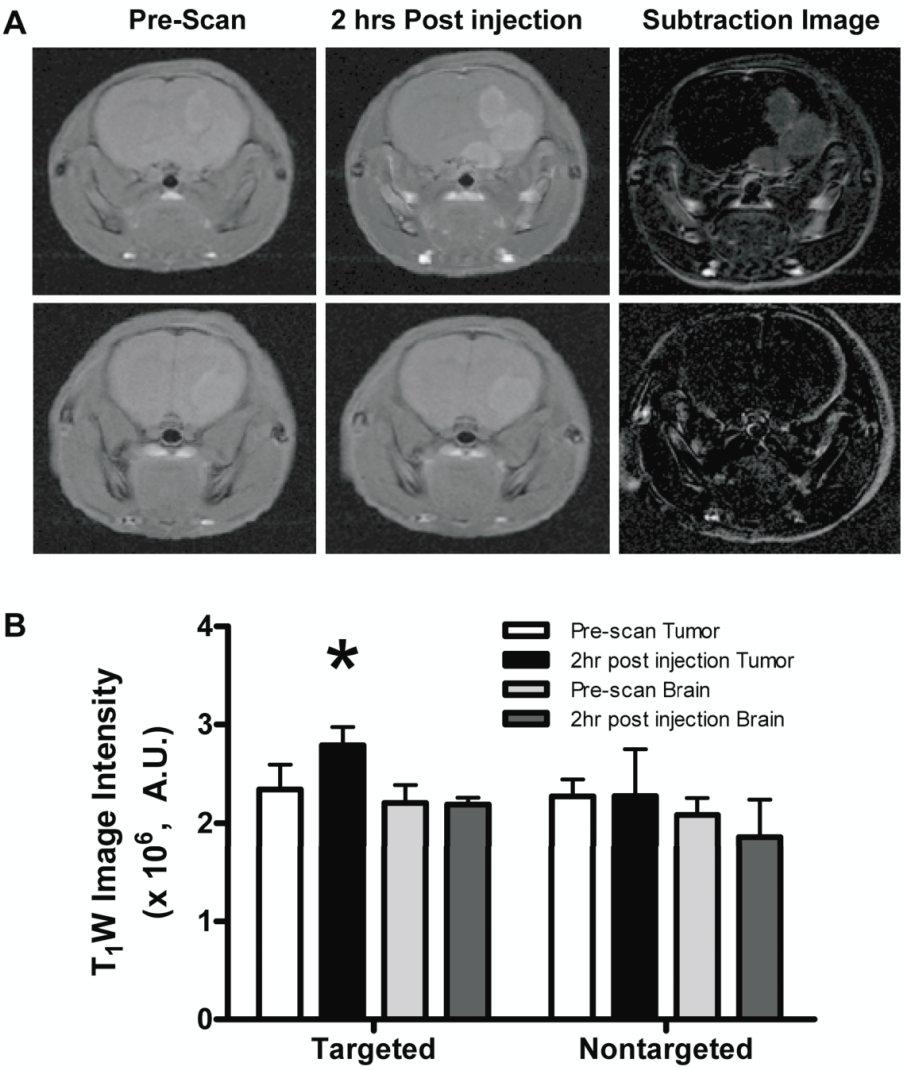

Figure 6. Enhanced MRI contrast of brain tumor region using anti-IGFBP7 sdAb targeted Gd-sULV. MRI of mice with brain tumors following injection of Gd loaded small unilamellar vesicles (Gd-sULVs). (A) T_1 weighted (T_1 w) images were acquired prior to and at 2 h following injection of either targeted anti-IGFBP7 sdAB labeled Gd-sULVs (upper panels) or nontargeted Gd-sULV's (lower panels). Subtraction images of the 2 h scan from pre-injection scan (A, right panels) show greater effects on T_1 w intensities in tumor with targeted compared to nontargeted contrast injection. (B) Intensity measures in tumor and contralateral brain resulted in mean differences in intensity that differed depending on region and time following targeted contrast injection ($p < 0.03$, Two-way ANOVA; * $p < 0.001$, paired comparison of brain versus tumor at 2 h) whereas differences following nontargeted contrast injection were not significant ($p > 0.4$, Two-way ANOVA).

both types of antibodies did demonstrate improved targeting compared to their nontargeted counterparts.

Targeting tumor cells or the tumor vasculature has been explored in a number of studies using molecular MRI (Kirpotin *et al* 2006, Sipkins *et al* 1998). Currently, the best studied targeting moieties for molecular MRI are $\alpha_v\beta_3$ integrin binding peptides (Sipkins *et al* 1998, Winter *et al* 2003). In a pivotal study by Sipkins *et al* (1998), which targeted the endothelial $\alpha_v\beta_3$ integrin using mAb targeted Gd loaded liposomes in a xenograft tumor model, MRI contrast in the tumor was not reached until ∼24 h. The half-life of the nanoparticles was reported to be ∼8 h. Long circulating Gd-liposomes (∼100–400 nm) are known to demonstrate slow accumulation in solid tumors even in the absence of targeting ligands (Drummond *et al* 2008) due to the enhanced permeability and retention (EPR) observed in xenograft tumor models (Vajkoczy *et al* 1998). Another study, (Kirpotin *et al* 2006), did not find increased tumor localization for anti-HER2 targeted lipids vesicles compared to their nontargeted lipid vesicles. The slow clearance of liposomes from the blood and the high background signal that is produced in the tumor by nontargeted lipid vesicles, due to the EPR effect (i.e. passive targeting), results in a reduced target to background signal (Mulder *et al* 2005). This makes the task of quantifying the contribution of active targeting difficult. In this study, anti-EGFR mAb targeted Gd-sULV did show an enhancement in targeting using optical imaging compared to nontargeted Gd-sULV, presumably due to the smaller size and shorter half-life compared to long circulating liposomes, contributing to less EPR. At the tissue level, the anti-EGFR mAb targeted

Gd-sULV results displayed increased cellular internalization, which is further evidence of active targeting processes. A limitation of this study is that the anti-EGFR mAb targeted Gd-sULV could have an increased half-life compared to its nontargeted counterpart due the presence of the Fc region (Roopenian and Akilesh 2007). This could also contribute to an increase in the level of targeting due to additional EPR effects. It is important to note that although the passive targeting associated with xenograft tumor models is essential for delivery of the contrast agents to the tumor cells, it can make the quantification of the degree of molecular targeting difficult.

To address these issues with anti-EGFR mAb, EGFR and xenograft tumors, a switch to the vascular target IGFBP7 and sdAbs in the more relevant orthotopic brain tumor model was investigated. The orthotopic brain tumor model in mice is characterized by the presence of the BTB, which limits the delivery of exogenous agents to the tumor (De Vries *et al* 2006). Targeting tumor vessels rather than tumor cells avoids the need to cross the BTB and interact with the tumor cells. Anti-IGFBP7 sdAb targeted Gd-sULVs demonstrated a high target to background signal with low passive accumulation of nontargeted Gd-sULVs in the orthotopic brain tumor model using optical imaging. The anti-IGFBP7 sdAb kept the Gd-sULV in the tumor vessels, whereas nontargeted Gd-sULVs did not accumulate in the tumor as a result of passive targeting effects, like in the xenograft tumor model. For molecular imaging, it is critical that the imaging signal from the tumor is primarily the result of active targeting related to antigen expression level and not passive targeting or nonspecific targeting (i.e. nonspecific cellular internalization). In this way, a more accurate measure of the molecular target can be assessed and quantified.

Another important parameter for MRI imaging with regards to the contrast agent is the amount of Gd loaded in the nanoparticle. In a study by Winter *et al* (2003), $\alpha_v\beta_3$ integrin targeted nanoparticle emulsions were reported to contain 90 000 Gd^{3+} ions per particle. This high payload of Gd per particle was considered important for increasing the signal to noise ratio (i.e., increased sensitivity). At only 2 h after the injection of the targeted nanoparticles, an increase in MRI contrast was observed compared to nontargeted nanoparticle emulsions. The effect at only 2 h was most likely associated with passive targeting due to the large ~250 nm size and long circulation half-life of the nanoparticle emulsion (>2 h). A drawback to nanoparticle emulsions, compared to sULVs or liposomes, is the processing required to produce the contrast agent and the resultant extended size distribution (i.e., 100–1000 nm) of the particles. In comparison, Gd-sULVs have the advantage of 30 000 Gd per nanoparticle (high payload), spontaneously forming and a narrow size distribution. In this study, the anti-IGFBP7 sdAb targeted Gd-sULV delivered a sufficient amount of Gd to the brain to produce a measurable contrast enhancement.

In another study that assessed molecular MRI of tumor vessels, anti-CD105 (endoglin) antibody targeted Gd-liposomes were used in an orthotopic brain tumor model in rat. Contrast enhancement was not observed in the intracranial model, but only in a xenograft brain tumor model (Zhang *et al* 2009). This lack of MRI contrast was attributed to low Gd liposome content or the quenching of the relaxivity of the Gd encapsulated inside the liposomal water compartment. MR contrast agents such as Gd produce their effects by affecting the MR relaxation of water within the sample. In the present study, T1 relaxivity of each Gd loaded sULV was much higher than that of free Gd-DTPA, and no evidence of quenching was observed when the Gd-DPTA was incorporated in the lipid bilayer. Another reason for the lack of contrast observed with an anti-CD105 targeted Gd-liposomes may have to do with the lack of specificity for tumor vessels, as endoglin is also expressed in normal vessels (Balza *et al* 2001). IGFBP7, however, is very selective for tumor vessels, with little or no expression in normal vessels (Iqbal *et al* 2010b, 2010a, Pen *et al* 2007).

The bimodal nature of the Gd-sULV-Cy5.5 contrast agent affords the benefits offered by both optical and MR imaging. Optical imaging provides high sensitivity, while MRI provides high anatomical resolution. In this study, it was apparent that optical imaging gave rise to a greater increase in tumor signal compared to that achieved using the less sensitive MRI. However, MRI provided highly detailed anatomical information, as it provides excellent contrast between different soft tissues, i.e. brain versus cancer. Co-registration of optical and MRI signals would thus take advantage of the intrinsic strengths of these modalities. In this study, optical imaging allowed for rapid pre-clinical optimization of the Gd-ULVs pharmacokinetic and biodistribution parameters before assessment in the more expensive MRI technique. Also, the fluorescence of the Gd-sULV-Cy5.5 nanoparticles allows one to study the molecular localization of the contrast agent using fluorescent microscopy in tissue sections.

In conclusion, the targeted contrast agent anti-IGFBP7 sdAb-Gd-sULV-Cy5.5 is a paramagnetic nanoscopic lipid vesicle that possesses an optimized pharmacokinetic profile for imaging, has high target avidity, due to the presence of multiple small sdAbs on its surface, possesses bimodal optical-MRI capabilities and carries a high payload of Gd for improved MRI detection sensitivity. Appropriate target selection is also a critical factor and requires careful case by case analysis. These features of Gd-sULV are the hallmarks for the future of MRI contrast agent.

Acknowledgments

The authors acknowledge P Forsyth, X Lun and D Rushforth's contribution to producing the mice tumor model, and T Foniok and D Kirk for their assistance with the acquisition of MR images using these mice. We would also like to thank D Fatehi for her assistance with cell culture experiments and T Devesceri for his help with graphic and image processing. The authors acknowledge the support of the National Institute of Standards and Technology, US Department of Commerce, in providing the neutron research facilities used in this work.

References

Abulrob A, Brunette E, Slinn J, Baumann E and Stanimirovic D 2007 *In vivo* time domain optical imaging of renal ischemia-reperfusion injury: discrimination based on fluorescence lifetime *Mol. Imaging* **6** 304–14

Abulrob A, Brunette E, Slinn J, Baumann E and Stanimirovic D 2008 Dynamic analysis of the blood-brain barrier disruption in experimental stroke using time domain *in vivo* fluorescence imaging *Mol. Imaging* **7** 248–62

Abulrob A, Giuseppin S, Andrade M F, McDermid A, Moreno M and Stanimirovic D 2004 Interactions of EGFR and caveolin-1 in human glioblastoma cells: evidence that tyrosine phosphorylation regulates EGFR association with caveolae *Oncogene.* **23** 6967–79

Arbabi Ghahroudi M, Desmyter A, Wyns L, Hamers R and Muyldermans S 1997 Selection and identification of single domain antibody fragments from camel heavy-chain antibodies *FEBS Lett.* **414** 521–6

Balza E, Castellani P, Zijlstra A, Neri D, Zardi L and Siri A 2001 Lack of specificity of endoglin expression for tumor blood vessels *Int. J. Cancer* **94** 579–85

Cai W and Chen X 2008 Multimodality molecular imaging of tumor angiogenesis *J. Nucl. Med.* **49** 113S–28S

De Schepper A M and Bloem J L 2007 Soft tissue tumors: grading, staging, and tissue-specific diagnosis *Top Magn. Reson. Imaging* **18** 431–333

De Vries N A, Beijnen J H, Boogerd W and van Tellingen O 2006 Blood-brain barrier and chemotherapeutic treatment of brain tumors *Expert Rev. Neurother.* **6** 1199–209

Drummond D C, Noble C O, Hayes M E, Park J W and Kirpotin D B 2008 Pharmacokinetics and *in vivo* drug release rates in liposomal nanocarrier development *J. Pharm. Sci.* **7** 4696–740

Glogard C, Stensrud G, Hovland R, Fossheim S L and Klaveness J 2002 Liposomes as carriers of amphiphilic gadolinium chelates: the effect of membrane composition on incorporation efficacy and *in vitro* relaxivity *Int. J. Pharm.* **233** 131–40

Glunde K, Pathak A P and Bhuiwalla Z M 2007 Molecular-functional imaging of cancer: to image and imaging *Trends Mol. Med.* **13** 287–97

Gupta H and Weissleder R 1996 Targeted contrast agents in MR imaging *Magn. Reson. Imaging Clin. N. Am.* **4** 171–84

Hamers-Casterman C, Atarhouch T, Muyldermans S, Robinson G, Hamers C, Songa E B, Bendahman N and Hamers R 1993 Naturally occurring antibodies devoid of light chains *Nature* **363** 446–8

Iqbal U, Albaghdadi H, Luo Y, Arbabi M, Desvaux C, Veres T, Stanimirovic D and Abulrob A 2010a Molecular imaging of glioblastoma multiforme using anti-insulin-like growth factor binding protein-7 single domain antibodies *Br. J. Cancer* **103** 1606–16

Iqbal U, Trojahn U, Albaghdadi H, Zhang J, O'Connor-McCourt M, Stanimirovic D, Tomanek B, Sutherland G and Abulrob A 2010b Kinetic analysis of novel mono- and multivalent VHH-fragments and their application for molecular imaging of brain tumours *Br. J. Pharmacol.* **160** 1016–28

Kirpotin D B, Drummond D C, Shao Y, Shalaby M R, Hong K, Nielsen U B, Marks J D, Benz C C and Park J W 2006 Antibody targeting of long-circulating lipidic nanoparticles does not increase tumor localization but does increase internalization in animal models *Cancer Res.* **66** 6732–40

Mahabir S, Wan W K, Katsaras J and Nieh M P 2010 The effects of charge density and thermal history on the morphologies of spontaneously formed unilamellar vesicles *J. Phys. Chem.* B **114** 5729–35

Mamot C, Drummond D C, Noble C O, Kallab V, Guo Z, Hong K, Kirpotin D B and Park J W 2005 Epidermal growth factor receptor-targeted immunoliposomes significantly enhance the efficacy of multiple anticancer drugs *in vivo Cancer Res.* **65** 11631–8

Michalski M H and Chen X 2011 Molecular imaging in cancer treatment *Eur. J. Nucl. Med. Mol. Imaging* **38** 358–7

Mulder W J, Strijkers G H, Habets J W, Bleeker E J, van der Schaft D W, Storm G, Koning G A, Griffioen A W and Nicolay K 2005 MR molecular imaging and fluorescence microscopy for indentification of activated tumor endothelium using a bimodal lipidic nanoparticle *FASEB J.* **14** 2008–10

Nagane M, Coufal F, Lin H, Bögler O, Cavenee W K and Huang H J 1996 A common mutant epidermal growth factor receptor confers enhanced tumorigenicity on human glioblastoma cells by increasing proliferation and reducing apoptosis *Cancer Res.* **56** 5079–86

Nieh M P, Harroun T A, Raghunathan V A, Glinka C J and Katsaras J 2003 Concentration independent spontaneously forming biomimetic vesicles *Phys. Rev. Lett.* **91** 158105

Nieh M P, Harroun T A, Raghunathan V A, Glinka C J and Katsaras J 2004 Spontaneously formed monodisperse biomimetic unilamellar vesicles: effect of charge, dilution and time *Biophys. J.* **86** 2615–29

Nieh M P, Katsaras J and Qi X 2008 Controlled release mechanisms of spontaneously forming unilamellar vesicles *Biochim. Biophys. Acta* **1778** 1467–71

Nieh M P, Raghunathan V A, Kline S R, Harroun T A, Huang C Y, Pence J and Katsaras J 2005 Spontaneously formed unilamellar vesicles with path dependent size distribution *Langmuir* **21** 6656–61

Pan D, Caruthers S D, Chen J, Winter P M, Senpan A, Schmider A H, Wickline S A and Lanza G M 2010 Nanomedicine strategies for molecular targets with MRI and optical imaging *Future Med. Chem.* **2** 471–90

Pen A, Moreno M J, Durocher Y, Deb-Rinker P and Stanimirovic D B 2008 Glioblastoma-secreted factors induce IGFBP7 and angiogenesis by modulating Smad-2-dependent TGF-beta signaling *Oncogene.* **27** 6834–44

Pen A, Moreno M J, Martin J and Stanimirovic D B 2007 Molecular markers of extracellular matrix remodeling in glioblastoma vessels: microarray study of laser-captured glioblastoma vessels *Glia* **55** 559–72

Sapra P, Moase E H, Ma J and Allen T M 2004 Improved therapeutic responses in a xenograft model of human B lymphoma (Namalwa) for liposomal vincristine versus liposomal doxorubicin targeted via anti-CD19 IgG2a or Fab' fragments *Clin. Cancer Res.* **10** 1100–11

Sipkins D A, Cheresh D A, Kazemi M R, Nevin L M, Bednarski M D and Li K C 1998 Detection of tumor angiogenesis *in vivo* by alphaVbeta3-targeted magnetic resonance imaging *Nat. Med.* **4** 623–6

Strijkers G J, Kluza E, Van Tilborg G A, van der Schaft D W, Griffioen A W, Mulder W J and Nicolay K 2010 Paramagnetic and fluorescent liposomes for target-specific imaging and therapy of tumor angiogenesis *Angiogenesis* **13** 161–73

Sulochana K N and Ge R 2007 Developing antiangiogenic peptide drugs for angiogenesis-related diseases *Curr. Pharm. Des.* **13** 2074–86

Roopenian D C and Akilesh S 2007 FcRn: the neonatal Fc receptor comes of age *Nat. Rev. Immunol.* **7** 715–25

Tassa C, Duffner J L, Lewis Y A, Weissleder R, Schreiber S L, Koehler A N and Shaw S Y 2010 Binding affinity and kinetic analysis of targeted small molecule-modified nanoparticles *Bioconjug. Chem.* **21** 14–9

Vajkoczy P, Schilling L, Ullrich A, Schmiedek P and Menger M D 1998 Characterization of angiogenesis and microcirculation of high-grade glioma: an intravital multifluorescence microscopy

approach in the athymic nude mouse *J. Cereb. Blood Flow Metab.* **18** 510–20

Winter P M *et al* 2003 Molecular imaging of angiogenesis in nascent Vx-2 rabbit tumors using a novel alpha(nu)beta3-targeted nanoparticle and 1.5 tesla magnetic resonance imaging *Cancer Res.* **63** 5838–43

Woodcock J and Woosley R 2008 The FDA critical path initiative and its influence on new drug development *Annu. Rev. Med.* **59** 1–12

Xu R, Wang Y, Wang X, Jeong E K, Parker D L and Lu Z R 2007 *In vivo* evaluation of a PAMAM-cystamine-Gd-DO3A conjugate as a biodegradable macromolecular MRI contrast agent *Exp. Biol. Med.* **232** 1081–9

Yue B, Huang C Y, Nieh M P, Glinka C J and Katasaras J 2005 Highly stable phospholipid unilamellar vesicles from spontaneous vesiculation: a DLS and SANS study *J. Phys. Chem.* **109** 609–16

Zhang D, Feng X Y, Henning T D, Wen L, Lu W Y, Pan H, Wu X and Zou L G 2009 MR imaging of tumor angiogenesis using sterically stabilized Gd-DTPA liposomes targeted to CD105 *Eur. J. Radiol.* **70** 180–9

Zhang R, Tremblay T L, McDermid A, Thibault P and Stanimirovic D 2003 Identification of differentially expressed proteins in human glioblastoma cell lines and tumors *Glia* **42** 194–208